Applied Catalysis B: Environmental 146 (2014) 201–212

Contents lists available at ScienceDirect

Applied Catalysis B: Environmental

journal homepage: www.elsevier.com/locate/apcatb

Efficient fabrication of active CuO-CeO_2/SBA-15 catalysts for preferential oxidation of CO by solid state impregnation

Changjin Tang[a], Jingfang Sun[a], Xiaojiang Yao[a], Yuan Cao[a], Lichen Liu[a], Chengyan Ge[a], Fei Gao[b,*], Lin Dong[a,b,*]

[a] Key Laboratory of Mesoscopic Chemistry of MOE, School of Chemistry and Chemical Engineering, Nanjing University, Nanjing 210093, PR China
[b] Jiangsu Key Laboratory of Emission Control, Center of Modern Analysis, Nanjing University, Nanjing 210093, PR China

ARTICLE INFO

Article history:
Received 24 September 2012
Received in revised form 25 April 2013
Accepted 23 May 2013
Available online 30 May 2013

Keywords:
Solid state impregnation
CuO-CeO_2
Interfacial interaction
CO-PROX
CO adsorption

ABSTRACT

A facile solid state impregnation method was reported to prepare CuO-CeO_2/SBA-15 catalysts for preferential oxidation of CO (CO-PROX). The catalysts were studied and compared with the counterpart from traditional wet impregnation. All catalysts together with a bulk CuO-CeO_2 were characterized by XRD, N_2 sorption, TEM, XPS, FT-IR of CO adsorption and H_2-TPR. Results showed that: (1) both copper and ceria were well dispersed on SBA-15, and by adoption of a supported CuO-CeO_2 configuration, the CO-PROX activities were greatly enhanced, which could be attributed to the distinct reduction of ceria size; (2) the optimum copper loading was 5 wt%, and obvious decrease of CO_2 selectivity was observed at higher loading; (3) in comparison with wet impregnation, the solid state impregnation displayed advantages of increased interfacial CuO-CeO_2 entities and enhanced interaction between CuO and CeO_2, which increased the active site and upgraded the CO-PROX activity resultantly. As well, the reason accounting for the different properties was tentatively discussed. On the basis of the preliminary results, it is supposed the solid state impregnation will find unique application in fabrication of multi-component heterogeneous catalysts.

1. Introduction

Preferential oxidation of CO (CO-PROX) has attracted numerous interests in recent years for its potential of avoiding poisoning of Pt-based anode in proton exchange membrane fuel cell (PEMFC) [1,2]. The key requirements for CO-PROX catalysts include extremely high CO oxidation activity, high selectivity, and wide operation window [3]. Supported Au and Pt catalysts are active for CO-PROX reaction, but they suffer from such drawbacks as high cost, limited availability and relatively low selectivity at high temperatures. Therefore, the development of non-precious catalysts with favorable performance is desirable.

Among the reported non-precious catalysts for CO-PROX, copper-ceria catalysts have gained tremendous attention [4–7]. In general, their activities are correlated with the synergetic effect between copper and ceria [6,8,9], and are intimately influenced by the adopted preparations. Chung and Yeh studied the effect of pH value on CuO/CeO_2 catalysts and found precipitation at high pH led to enhanced interaction between copper and ceria, which increased the CO-PROX activity [10]. Lee and co-workers investigated the impact of hydrothermal treatment after co-precipitation procedure on the property of CuO/CeO_2 catalyst. They found that under hydrothermal process, cuprous ions would migrate to the surface of the catalyst resulting in increased concentration of interfacial copper-ceria entities. As a consequence, improved CO conversion was obtained [11].

In addition to preparation parameters, the activity of CuO-CeO_2 catalysts over CO-PROX is reported to be also affected by their configurations [12]. Commonly, the configurations of CuO-CeO_2 catalysts can be classified into three kinds, *i.e.*, CuO/CeO_2, inverse CeO_2/CuO and supported CuO-CeO_2. In contrast to the overwhelming investigations on CuO/CeO_2, little attention has been paid to the application of supported CuO-CeO_2, despite their favorable performances. Chilukuri and co-workers studied the possibility of using Al-pillared montmorillonite (Al-PILC) clay as a support for CuO-CeO_2 catalysts [13] and result showed that the CuO-CeO_2/Al-PILC catalysts were comparable to supported noble metal catalysts in the performance of CO-PROX. Araya and co-workers put their attention on the effect of various supports (Al_2O_3, ZrO_2 and SiO_2) on CuO-CeO_2 catalysts and pointed out that the employed supports exerted a critical influence on the interaction degree between copper and ceria, and consequently the CO-PROX activity, with CuO-CeO_2 supported on SiO_2 displaying the best CO oxidation activity [14].

* Corresponding authors at: Jiangsu Key Laboratory of Emission Control, Center of Modern Analysis, Nanjing University, Nanjing 210093, PR China.
Tel.: +86 25 83592290; fax: +86 25 83317761.
E-mail addresses: gaofei@nju.edu.cn (F. Gao), donglin@nju.edu.cn (L. Dong).

0926-3373/$ – see front matter © 2013 Elsevier B.V. All rights reserved.
http://dx.doi.org/10.1016/j.apcatb.2013.05.060

For supported CuO-CeO_2 catalysts, the effective interaction between copper and ceria is vital. It is properly supposed that by adopting a suitable method, the interaction between copper and ceria on the third support would be altered, which dictates their final performance. So far, methods for dispersing multiple components onto a support are dominated by wet impregnation, whereas the investigations of other methods are seldom reported and the direct comparison between them is lacking. Recently, a typical method featuring of solid state impregnation was reported by others [15,16] and performed in our laboratory [17], and unique capacity in dispersion was achieved for mono-component species supported on mesoporous SBA-15. Actually, in many catalyst systems, in addition to the support and active component, a promoter or modifier is usually added to obtain certain desirable properties (*e.g.* improved activity, selectivity, thermal stability, and poison resistance). In that case, the interactions between active species, promoter as well as support are complex, and the capacity of solid state impregnation in distributing guest species and modulating their interactions is still a question of great interest. Moreover, because of the complexity of the systems, it is still unclear how copper and ceria interact with each other and how such interaction promotes catalytic activities. Hence, in the present study, as an alternative to wet impregnation, we extend the solid state impregnation to fabricate CuO-CeO_2/SBA-15 catalysts. The main focus of the present study is to: (1) investigate the effectiveness of solid state impregnation in preparing SBA-15 supported copper-ceria catalysts; (2) explore the differences in the composition and structure of the catalysts made by solid state impregnation and wet impregnation, and correlate them with the CO-PROX activity. The characterization results reveal that both CuO and CeO_2 are well dispersed and the interaction between copper and ceria can be enhanced *via* the solid state impregnation. As a result, the obtained catalysts display superior performance in CO-PROX, in comparison with bulk CuO-CeO_2 and CuO-CeO_2/SBA-15 from wet impregnation.

2. Experimental

2.1. Preparation of catalyst

2.1.1. Preparation of SBA-15 supported CuO-CeO_2 catalysts by solid state impregnation

All chemicals used in the experiments were of analytical grade, and were used without further purification. Synthesis of SBA-15 follows Zhao's process [18]. The solid state impregnation to CuO-CeO_2/SBA-15 catalysts was operated as follows. A certain amount of $Ce(NO_3)_3{\cdot}6H_2O$ and $Cu(NO_3)_2{\cdot}3H_2O$ were added to an agitate mortar with SBA-15 and manually ground for 0.5 h. Then the mixed powder was transferred into a crucible, which was placed in the muffle furnace. The thermal treatment in air started at room temperature with a ramp of 1 °C min^{-1} to 450 °C and maintained at that temperature for 4 h, then cooled naturally. For simplicity, the obtained samples were denoted as *x*CuCe/SBA-15-SSI, where ceria content was set to 20 wt% and *x* represented the weight percentage of CuO to SBA-15. As well, 5Cu/SBA-15-SSI was prepared by the same procedure.

2.1.2. Preparation of SBA-15 supported CuO-CeO_2 catalyst by wet impregnation method

The supported CuO-CeO_2 catalyst from wet impregnation was prepared by impregnating SBA-15 with an aqueous solution containing requisite amount of $Ce(NO_3)_3{\cdot}6H_2O$ and $Cu(NO_3)_2{\cdot}3H_2O$. After stirred for 2 h, the sample was dried at 100 °C in oil bath, subsequently dried at 110 °C in an oven overnight, and then calcined in air at 450 °C for 4 h. The obtained catalyst was denoted as 5CuCe/SBA-15-WI, and the copper and ceria contents are identical to that in 5CuCe/SBA-15-SSI.

2.1.3. Preparation of bulk CuO-CeO_2 catalyst

As a representative of commonly employed copper-ceria configuration, CuO/CeO_2 catalyst was fabricated for comparison. The nominal ratio of CuO to ceria was set identical to that in 5CuCe/SBA-15-SSI, *i.e.*, CuO:CeO_2 = 1:4 (w/w). The catalyst was prepared by a co-precipitation method and noted as bulk CuCe. Typically, an aqueous solution of NaOH (1 M) was added dropwise to an aqueous mixture solution of cupric nitrate and cerium nitrate under stirring, and the pH of the finally resulted solution was controlled to *ca.* 10. After continued stirring for 3 h followed by aging for another 3 h, the resulted precipitate was filtered, washed with distilled water for several times, and dried at 110 °C overnight. Finally, the precipitate was air-calcined at 450 °C for 4 h.

2.2. Characterization of catalyst

The CuO and ceria contents in CuO-CeO_2/SBA-15 catalysts were determined by a Jarrell-Ash 1100 inductively coupling plasma (ICP) atomic emission spectrometer. The samples were completely dissolved in the mixed hot solutions of HF and H_2O_2 before analysis. The actual contents are equal to their nominal loadings.

X-ray diffraction (XRD) patterns were recorded on a Philips X'Pert Pro diffractometer, equipped with a Ni-filtered Cu Kα radiation (λ = 0.15418 nm). The X-ray tube was operated at 40 kV and 40 mA. The average grain size was determined from XRD line broadening measurement using the Scherrer equation, $d = K\lambda/\beta\cos\theta$, where λ is the X-ray wavelength, θ is the diffraction angle, K is the particle shape factor, usually taken as 0.89, and β is full width at half maximum in radians.

Nitrogen physisorption isotherms were measured at −196 °C using a Micromeritics ASAP 2020 system. The samples were degassed for 160 min at 300 °C in the degas port of the adsorption analyzer. The pore size distributions were calculated from the adsorption branch of the isotherm using the Barrett–Joyner–Halenda (BJH) algorithm.

Transmission electron microscopy (TEM) images were taken on a JEM-2100 instrument at an acceleration voltage of 200 kV. The sample was dispersed in A.R. grade ethanol with ultrasonic treatment and the resulting suspension was allowed to dry on carbon film supported on copper grids.

H_2 temperature-programmed reduction (H_2-TPR) measurement was carried out in a quartz U-tube reactor. Before reduction, the samples were pretreated in N_2 stream at 150 °C for 1 h and then cooled to room temperature. After that, a H_2-Ar mixture (7% H_2 by volume) with a flow rate of 70 mL min^{-1} was switched on and the temperature was increased linearly at a rate of 10 °C min^{-1}. A thermal conductivity cell was used to detect the consumption of H_2 on stream.

X-ray photoelectron spectroscopy (XPS) was performed on a PHI 5000 Versaprobe system, using monochromatic Al Kα radiation (1486.6 eV) operating at an accelerating power of 150 W. The samples were outgassed at room temperature in a UHV chamber ($<5 \times 10^{-7}$ Pa). All binding energies (B.E.) were referenced to the C 1s peak at 284.6 eV. The experimental errors were within ±0.1 eV.

FT-IR spectra were collected on a Nicolet 5700 FT-IR spectrometer at a resolution of 4 cm^{-1}. The spectra of empty IR cell were collected in CO atmosphere at various target temperatures as background. The catalysts were mounted in a commercial controlled environment chamber (HTC-3) and pretreated for 1 h at 150 °C in flowing N_2 atmosphere. After cooled to room temperature, the sample wafers were exposed to a controlled stream of CO-Ar (10% of CO by volume) at a rate of 5.0 mL min^{-1} for 30 min. Adsorption studies were performed by heating the adsorbed species and the spectra

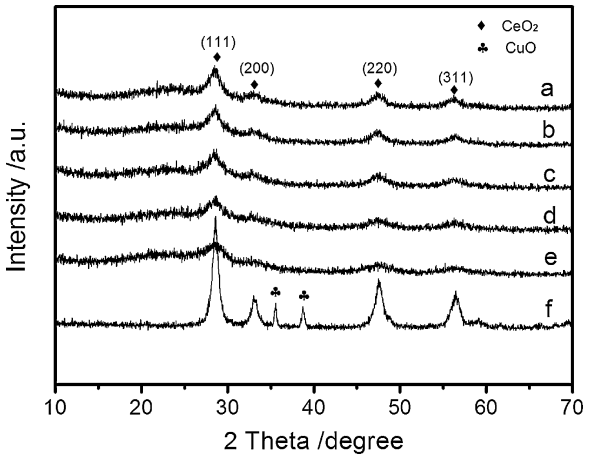

Fig. 1. XRD patterns of various copper-ceria catalysts. (a–d) *x*CuCe/SBA-15-SSI with copper contents of (a) 1 wt%, (b) 3 wt%, (c) 5 wt%, (d) 10 wt%, (e) 5CuCe/SBA-15-WI and (f) bulk CuCe.

were recorded at target temperatures. All of the presented spectra were obtained by subtraction of the corresponding background reference.

2.3. Catalytic tests

The activities of CuO-CeO_2 catalysts in CO-PROX reaction were measured in a flow, fixed-bed micro-reactor at atmospheric pressure. The reactor was a 3 mm i.d. (5 mm o.d., length 40 cm) quartz cube housed in a furnace. The catalyst temperatures were measured with a K-type thermocouple inserted in the middle of the catalyst bed. The reaction gas composition is 1.0 vol% CO, 1.0 vol% O_2, 50 vol% H_2, 10 vol% H_2O (when used), 15 vol% CO_2 (when used) with N_2 as balance gas. The total flow rate of the reactants was kept constant at 30 mL min^{-1} and the used amount of catalyst was 100 mg (for bulk CuCe, 20 mg catalyst was diluted with 80 mg quartz sand to equalize the CuO-CeO_2 utilization). The catalysts were pretreated in a N_2 stream at 150 °C for 1 h before switched to the reaction gas stream.

The reactor inlet and outlet streams were measured using an on-line gas chromatograph (Shimadzu GC-14C) equipped with a thermal conductivity detector (TCD) and a flame ionization detector (FID). CO, O_2 and N_2 were separated by a 5A molecular sieve column and detected using TCD. CO was converted to methane by a methanation reactor and analyzed by FID. The CO conversion (X_{CO}) and selectivity to CO_2 (S_{CO}) in excess hydrogen were calculated as follows:

$$X_{CO}(\%) = \frac{[CO]_{in} - [CO]_{out}}{[CO]_{in}} \times 100 \quad (1)$$

$$S_{CO_2}(\%) = \frac{0.5([CO]_{in} - [CO]_{out})}{[O_2]_{in} - [O_2]_{out}} \times 100 \quad (2)$$

3. Results and discussion

3.1. XRD

Fig. 1 shows the XRD patterns of CuO-CeO_2/SBA-15 and bulk CuO-CeO_2 catalysts. It is clear that all samples from solid state impregnation (profiles a–d) display only characteristic diffraction peaks of fluorite CeO_2 (JCPDS #43-1002), without diffraction peaks due to copper species, even when 10 wt% CuO is introduced. The results indicate that copper species are highly dispersed. Moreover, the intensities of ceria diffraction peaks are slightly weakened with increasing of copper contents, suggesting interplay between copper and ceria and a decline in crystallite size of CeO_2 are happened [6,19]. Detailed analysis of line broadening by Sherrer equation provides the mean grain sizes of ceria in the samples (Table 1). It can be seen that all ceria in *x*CuCe/SBA-15-SSI are smaller than 5 nm and increasing copper content to 10 wt% leads to ceria with tiny size of *ca.* 3.8 nm.

On the other hand, by comparing the profile of 5CuCe/SBA-15-SSI with those of 5CuCe/SBA-15-WI and bulk CuCe (profiles c, e, f), it is shown that the diffractions of CuO-CeO_2 catalysts are much affected by their configurations, whereas the impact of preparation methods is not significant. Both diffraction peaks attributed to fluorite ceria and tenorite (JCPDS #03-0884) are obvious for bulk CuCe (profile f), implying CeO_2 particles are well crystallized and CuO content (20 wt%) largely exceeds the dispersion capacity of ceria [20]. For 5CuCe/SBA-15-WI, similar diffractions to that of 5CuCe/SBA-15-SSI are observed, *i.e.*, appearance of broad ceria peaks and absence of copper oxide peaks. By close inspection, it is found that ceria size is weakly influenced by the preparation methods, with wet impregnation attaining slightly smaller size. From XRD result, it can be facilely concluded: (1) the presence of solvent is not requisite for dispersing guest species onto a support. As an alternative to conventional wet impregnation, the present solid state impregnation can effectively disperse copper species and ceria onto SBA-15; (2) the employment of SBA-15 is favorable for reduction of ceria size. Besides, in consideration of the thermal treatment at 450 °C for 4 h, the rigid support can simultaneously impart ultrafine ceria with certain thermal stability.

3.2. TEM

The size and dispersion of ceria are further explored by TEM characterization. For bulk CuCe (Fig. 2a), the ceria are composed of weakly aggregated particles with irregular shape and rough surface. Their particle sizes acquire 8–20 nm, which is in line with the calculated average size (11.2 nm) from XRD result and proves they are primary particles. For CuO-CeO_2/SBA-15 catalysts, the one-dimension pore channels are visible in the low resolution images (Fig. 2b and c), implying preservation of ordered mesostructures after introduction of guest species. This is also supported by the appearance of three diffraction peaks in low angle XRD results (see Fig. S1 in supporting information). Besides, numerous dark dots with size smaller than 5 nm are discerned and they are well scattered on the support. To check the nature of these dots, the high resolution TEM image is taken (Fig. 2d). The crystalline nature of these tiny particles is validated by appearance of multiple periodic lattice fringes, and the interplanar spacing of 0.32 nm is compatible with the expected distance between (1 1 1) planes of cubic ceria. It verifies the scattered dots are ceria crystallites. For copper species, no evidence of crystalline CuO is detected and it is in line with XRD result and further confirms they are highly dispersed.

3.3. N_2 physisorption

To disclose the textual characteristic of the prepared catalysts, N_2 sorption measurement is performed. In general, it can be seen from Fig. 3a that all isotherms are of type IV accompanied by an H_1 hysteresis loop according to IUPAC classification, confirming the existence of ordered one dimensional mesopores [21]. By comparing the isotherms of *x*CuCe/SBA-15-SSI and 5CuCe/SBA-15-WI with that of SBA-15, one distinction is observed. After introduction of CuO and ceria, an obvious two-step capillary evaporation with forced closure of hysteresis loop around $p/p^0 = 0.42$ appears. The phenomenon is typical of pore-plugging [22,23] and it indicates that partial straight channels are filled by guest species. As copper species are highly dispersed, the blockage of mesopores is

Table 1
The particle sizes, textural properties and chemical compositions of CuO-CeO_2/SBA-15 and bulk CuO-CeO_2 catalysts.

Sample	D^a (nm)	S^b (m^2/g)	V^c (cm^3/g)	Bulk composition[d]		Surface composition[e]		Ce^{3+} (%)	I_{sat}/I_{main}
				CuO (wt%)	CeO_2 (wt%)	CuO (wt%)	CeO_2 (wt%)		
1CuCe/SBA-15-SSI	4.4	565.3	0.64	1.02	20.5	–	9.6	21.4	–
3CuCe/SBA-15-SSI	4.4	548.0	0.62	3.04	20.3	–	10.6	22.0	–
5CuCe/SBA-15-SSI	4.3	539.8	0.62	4.98	19.8	1.1	8.9	24.8	0.54
10CuCe/SBA-15-SSI	3.8	487.5	0.54	10.6	20.1	3.9	12.6	22.6	0.66
5CuCe/SBA-15-WI	3.9	562.4	0.66	5.10	20.2	4.4	11.6	21.7	0.70
bulk CuCe	11.2	69.0	0.17	20.7	79.3	20.9	79.1	14.6	0.77
SBA-15	–	801.0	1.01	–	–	–	–	–	–

[a] Average particle size of ceria.
[b] Surface area.
[c] Pore volume.
[d] Bulk composition determined by ICP.
[e] Surface composition determined by XPS.

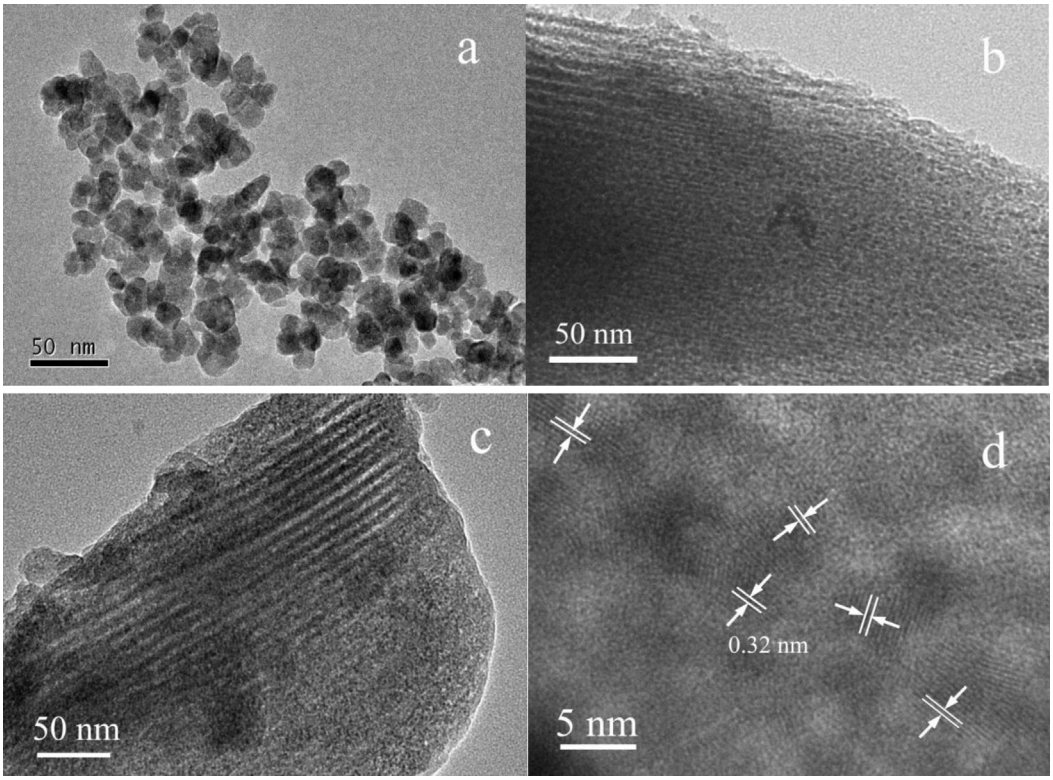

Fig. 2. TEM images of representative samples. (a) bulk CuCe, (b) 5CuCe/SBA-15-WI and 5CuCe/SBA-15-SSI with (c) low and (d) high magnification.

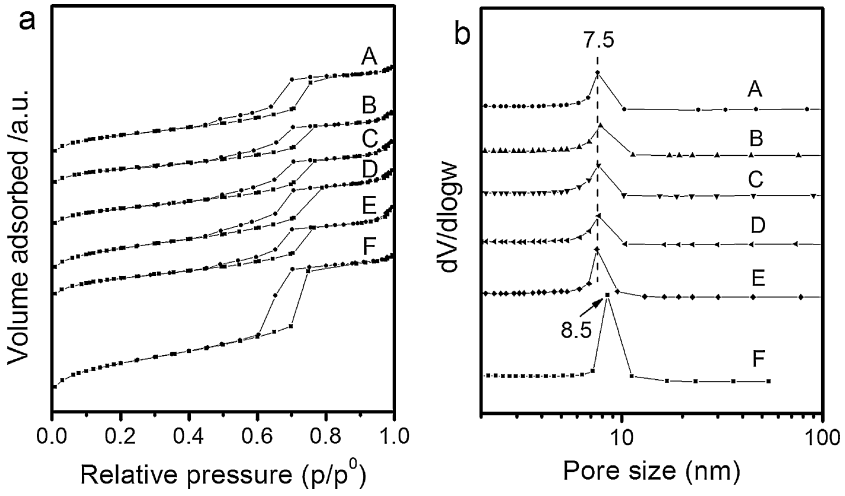

Fig. 3. N_2 sorption isotherms and pore size distributions of varied samples. (A–D) *x*CuCe/SBA-15-SSI with copper contents of (A) 1 wt%, (B) 3 wt%, (C) 5 wt%, (D) 10 wt%, (E) 5CuCe/SBA-15-WI and (F) pristine SBA-15.

probably caused by insertion of nanosized ceria particles. The location of ceria in the mesopores can be also deduced from the pore size distribution results. From Fig. 3b, it can be clearly observed that after introduction of copper and ceria, the pore sizes are decreased in comparison with pristine SBA-15. Moreover, the pore sizes of CuO-CeO_2/SBA-15 are almost independent of copper loadings, suggesting the reduction of pore size is mainly caused by ceria occupation in mesopores.

The textual parameters of CuO-CeO_2 catalysts derived from N_2 sorption are filed in Table 1. For bulk CuCe, the surface area and pore volume are relatively small with values of 69.0 m^2/g and 0.17 cm^3/g, respectively. It is reasonable to understand that with involvement of SBA-15, the values are significantly increased. Nevertheless, the surface areas and pore volumes of *x*CuCe/SBA-15-SSI and 5CuCe/SBA-15-WI are still much smaller than that of pristine SBA-15, which further verifies ceria are inserted into the mesopores and cause the occupation of void space of mesopores. For *x*CuCe/SBA-15-SSI with different copper contents, both pore volumes and surface areas are not much changed within lower copper contents (≤5 wt%), which is in agreement with the high dispersion nature of copper species. However, when higher copper (10 wt%) is introduced, both parameters are evidently decreased, indicating distinct interaction between copper species and silica is probably occurred and causes partial destruction of pore structure. This is in good agreement with the low angle XRD result (Fig. S1). For the samples from different methods (5CuCe/SBA-15-SSI and 5CuCe/SBA-15-WI), it is notable that their surface areas and pore volumes are similar, suggesting comparable textural properties of the two 5 wt% CuO loaded catalysts.

On the basis of the above characterizations, it is known that the solid state impregnation can comparably disperse copper and ceria as wet impregnation. In principle, the primary states related to ceria are established (ceria size: *ca.* 4 nm, ceria position: confined in mesopores), whereas the information about copper species is still obscure. Thus, to further disclose the states of copper species, *e.g.* their valence, location and relative content on the supports, such characterizations like XPS, FT-IR of CO adsorption and H_2-TPR are carried out.

3.4. XPS

XPS characterization is performed to approach the surface composition and chemical state of elements existing in catalysts. For CuO-CeO_2/SBA-15, it is found that the surface concentrations of copper and ceria are much lower than their bulk contents as determined by ICP (Table 1). This phenomenon is supposed to be related to pore confined effect. Due to the limited detection depth of photoelectron (<2 nm), some copper and ceria in the mesopores may not be detected with the shielding of silica skeleton. As a result, the signal is only partially collected. For the lower copper loaded samples (1CuCe/SBA-15-SSI and 3CuCe/SBA-15-SSI), copper signals can hardly be noticed as shown in Fig. 4c. For the higher copper loaded samples (10CuCe/SBA-15-SSI), it is observed that the copper concentrations are 2.5 times higher than that in 5CuCe/SBA-15-SSI, suggesting more copper are distributed on the exterior surface of SBA-15. Moreover, the much higher surface copper concentrations acquired by 5CuCe/SBA-15-WI indicates that in comparison with solid state impregnation, the wet impregnation is likely to disperse more copper species outside of mesopores.

The spectra of O 1s, Ce 3d and Cu 2p are displayed in Fig. 4. In general, the peak intensities of cerium and copper in CuO-CeO_2/SBA-15 catalysts are much weaker than those in bulk CuCe, which can be reasonably attributed to the reduced concentrations after importing of SBA-15. For O 1s spectra, it is apparent that two O 1s peaks are included in CuO-CeO_2/SBA-15 catalysts (Fig. 4a), with the main peak at higher binding energy (532.4 eV) attributed to —OH on the surface of SBA-15 and the shoulder peak at 528.9 eV to characteristic lattice oxygen of metal oxides [24]. Owing to absence of abundant surface silica hydroxyl, the spectrum of bulk CuCe is changed, with O 1s signal dominated by lattice oxygen at 528.7 eV. Additionally, there are two broad peaks at 532.4 eV and 530.6 eV, which can be assigned to oxygen from surface adsorbed carbonate and hydroxyl groups [24], respectively.

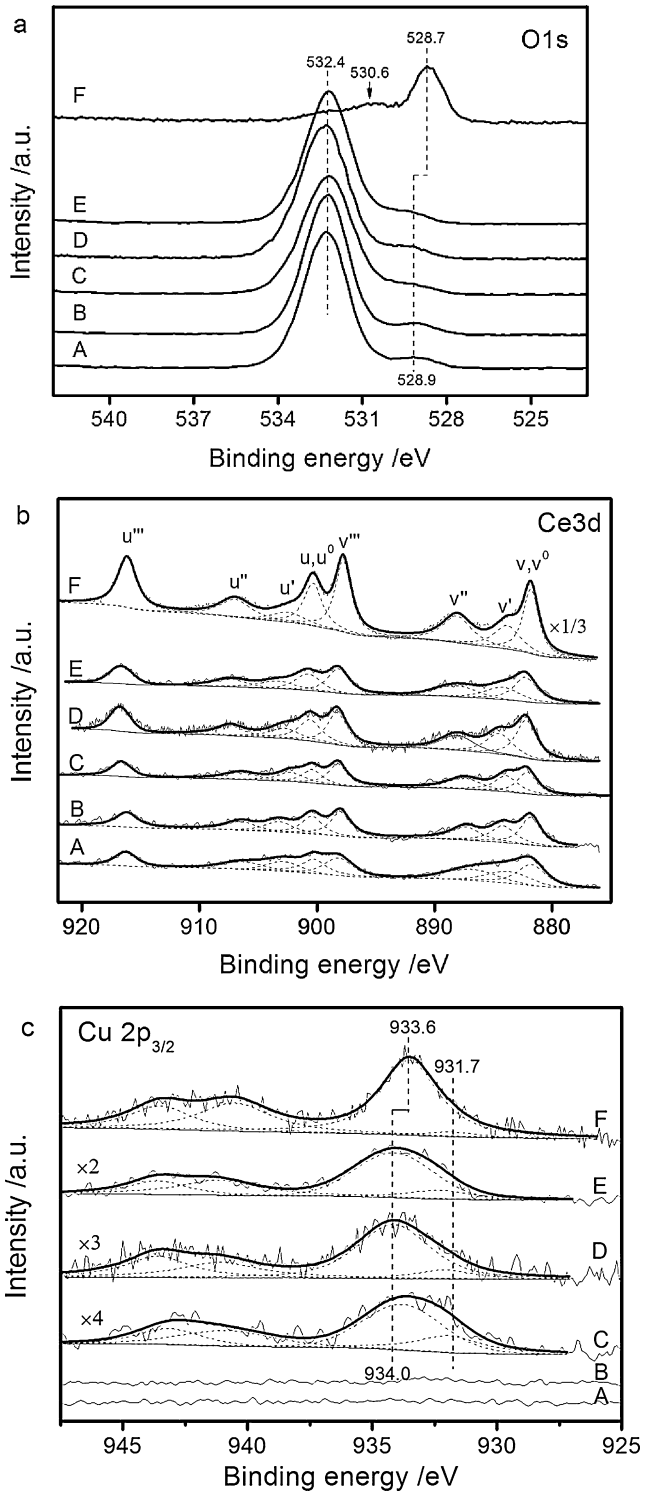

Fig. 4. XPS spectra of (a) O 1s, (b) Ce 3d and (c) Cu 2p for various samples. (A–D) *x*CuCe/SBA-15-SSI with copper contents of (A) 1 wt%, (B) 3 wt%, (C) 5 wt%, (D) 10 wt%, (E) 5CuCe/SBA-15-WI and (F) bulk CuCe.

The complex spectra of Ce 3d are shown in Fig. 4b and decomposed according to reference [25]. The nonlinear curve-fitting process is performed by using Xpspeak41 software package and the assignment are defined. Two sets of spin-orbital multiplets, corresponding to the $3d_{3/2}$ and $3d_{5/2}$ contributions, are labeled as *u* and *v*, respectively. The chemical valence of cerium on the surface of these samples is mainly in +4 oxidation state (*u*‴, *v*‴), and a small amount of Ce^{3+} (*u*′, *v*′) co-exists [26]. A favorable method, considering the relative integrated areas of *u*′ and *v*′ to the total bands, is applied to estimate Ce^{3+} [25,27] and the results are listed in Table 1. For bulk CuCe, the percentage of Ce^{3+} is 14.6% and comparable to the reported value [28]. Obviously, enlargement of Ce^{3+} concentration is detected when supported CuO-CeO_2 configuration is involved. Recently, increasing attention had been paid to the size-dependent properties of nanoscale ceria. It was reported that for ceria nanopartilces of 2–10 nm, stabilization of Ce^{3+} defects on the surface was obvious and the ratio of Ce^{3+}/Ce^{4+} increased with particle size decreasing [25,29]. This can explain well the higher Ce^{3+} concentrations in CuO-CeO_2/SBA-15 catalysts. However, despite owning smaller ceria size, the 5CuCe/SBA-15-WI sample displays less Ce^{3+} than that in 5CuCe/SBA-15-SSI, which conveys that some extrinsic factors instead of ceria size influence the evolution of Ce^{3+}. As a matter of fact, metal ions doping in ceria lattice (*e.g.*, La^{3+}, Zr^{4+}) is a common method to induce generation of oxygen vacancy and spontaneous transformation of Ce^{4+} into Ce^{3+} [30–32]. Thus, the higher Ce^{3+} concentration in 5CuCe/SBA-15-SSI suggests partial copper ions are doped into ceria and induce additional Ce^{3+}. Importantly, in comparison with simple pure ceria support, it was proved that the using of metal doped ceria as a support could decrease the energy for oxygen activation and facilitate reduction of surface-dispersed copper oxide, which promoted CO oxidation preferentially [6,32].

As for copper species, the spectra are shown in Fig. 4c. It can be safely concluded that most Cu are in +2 oxidation state, which is substantiated by the well fitted main peaks of Cu $2p_{3/2}$ at 933.6 and 934.0 eV for bulk CuCe and CuO-CeO_2/SBA-15, respectively. They are in accordance with the standard binding energy of Cu $2p_{3/2}$ for CuO (933.4–934.0 eV) [33]. Moreover, the appearance of well-marked satellite peak characteristic of Cu^{2+} at 937.8–947.5 eV supports the conclusion.

Previously, there were reports proposed that due to facile electron transfer between copper and ceria, some reduced copper species, *i.e.* Cu^{+}, were induced in copper-ceria catalyst system *via* the following redox process [34]:

$$Ce^{3+} + Cu^{2+} \rightarrow Ce^{4+} + Cu^{+}$$

In the present case, the existence of reduced copper is verified by a weak peak at lower binding energy (*ca.* 931.7 eV). It is reported that the lower Cu $2p_{3/2}$ binding energy and absence of the satellite peaks are characteristic of reduced copper species. By comparing the ratio of intensities of satellite peaks to those of main peaks (I_{sat}/I_{main}), the estimation of reduced copper species is acquired and result is listed in Table 1. Due to the photoreduction in the spectrometer, it is difficult to obtain the accurate reduction degree of Cu species, but this method gives valuable information for comparison among samples. It is apparent that CuO-CeO_2/SBA-15 catalysts display smaller I_{sat}/I_{main} values than that of bulk CuCe. Besides, the I_{sat}/I_{main} value for 5CuCe/SBA-15-SSI is lower in comparison with 5CuCe/SBA-15-WI. Thus, the direct comparison of ratio of peak intensities suggests higher content of reduced copper species (mainly Cu^{+}) is induced in 5CuCe/SBA-15-SSI, which is in agreement with the higher Ce^{3+} concentration and shows more facile redox cycle between copper and ceria. This can be viewed as a good indication of enhanced synergetic interaction between copper and ceria *via* solid state impregnation.

3.5. FT-IR of CO adsorption

To further investigate the state of copper species, we employ CO as a probing molecule and record its adsorption on the catalysts (Fig. 5). The spectra of CuO-CeO_2/SBA-15 catalysts (Fig. 5a–e) present several similar features in the selected range: (1) all spectra are dominated by two bands with vibration frequencies at 2130 cm^{-1} and around 2110 cm^{-1}, and the intensity of bands is actually a function of temperature; (2) the bands around 2130 cm^{-1} are only a weak peak at room temperature for all catalysts, but their signals intensify with temperature increasing. Moreover, their vibration frequencies almost keep constant with the increase of temperature; (3) contrarily, the bands around 2110 cm^{-1} are evident at room temperature, and the signals follow the changes of initial intensification and then gradual weakening or even disappearing with elevating of temperatures.

As pure ceria do not give any signal of CO adsorption above room temperatures, the bands shown in Fig. 5 reflect the adsorption of CO on copper species. According to literature [35], the adsorptions of CO molecules on Cu^{2+}, Cu^{+} and Cu^{0} give rise to peaks with characteristic vibration frequencies at about 2150–2220 cm^{-1}, 2080–2160 cm^{-1}, and below 2130 cm^{-1}, respectively. Among these, the most stable is Cu^{+}-carbonyl (Cu^{+}–CO). Thus, it is reasonable to suggest that the bands at 2080–2160 cm^{-1} in the present spectra correspond to vibration of CO molecules adsorbed on Cu^{+}. These Cu^{+} species contain both intrinsic and newly generated Cu^{+} *via* gradual reduction of Cu^{2+} with CO [36]. Previously, Hadjiivanov and Vayssilov had reviewed adsorption of CO on Cu-based catalysts and pointed out that CuO supported on various supports gave different vibration frequencies of CO adsorption [35]. For CuO/SiO_2 system, the adsorption of CO resulted in a typical band between 2128 and 2140 cm^{-1}. This triggers us to suppose that the band at 2130 cm^{-1} is arrived from copper species dispersed on SBA-15. To prove this assumption, we perform CO adsorption on 5Cu/SBA-15-SSI (Fig. 5f). As expected, the CO adsorption of 5Cu/SBA-15-SSI only gives a band with invariable wavenumber at 2130 cm^{-1} and its intensity is enhanced with temperature increasing. The result shows us indubitable evidence that in the SBA-15 supported copper-ceria catalysts, some copper species are dispersed on silica matrix.

The simultaneous appearance of two bands for CO adsorption is interesting and deserved to be noted. It is supposed that the bands are arrived from copper species dispersed on different supports. This is in full coincidence with the fact that only two possible types of dispersed copper species exist, *i.e.*, supported on silica or ceria. Moreover, both the location and evolution of signal with temperature are very similar with the referred spectra of bulk CuO/CeO_2 (Fig. 5f), which provides powerful evidence that some copper species are attached on ceria.

The CO adsorption result qualitatively shows copper species in CuO-CeO_2/SBA-15 catalysts are dispersed on both SBA-15 and ceria. However, the quantitative aspect of copper species is still not quite clear. In order to further investigate the relative amount of CuO dispersed on both carriers, *i.e.* ceria and SBA-15, the H_2-TPR characterization is carried out.

3.6. H_2-TPR

The H_2-TPR results of SBA-15 supported copper-ceria catalysts are shown in Fig. 6. As references, the profiles of 5Cu/SBA-15-SSI and bulk CuCe samples are also listed. The reduction of copper species on SBA-15 is represented by 5Cu/SBA-15-SSI shown in Fig. 6a. It can be seen that there is only one intense peak with maximum H_2 consumption at 202 °C. This value is smaller than what is expected for reduction of crystalline CuO (~300 °C) and consistent with its high dispersion nature. The reduction behavior

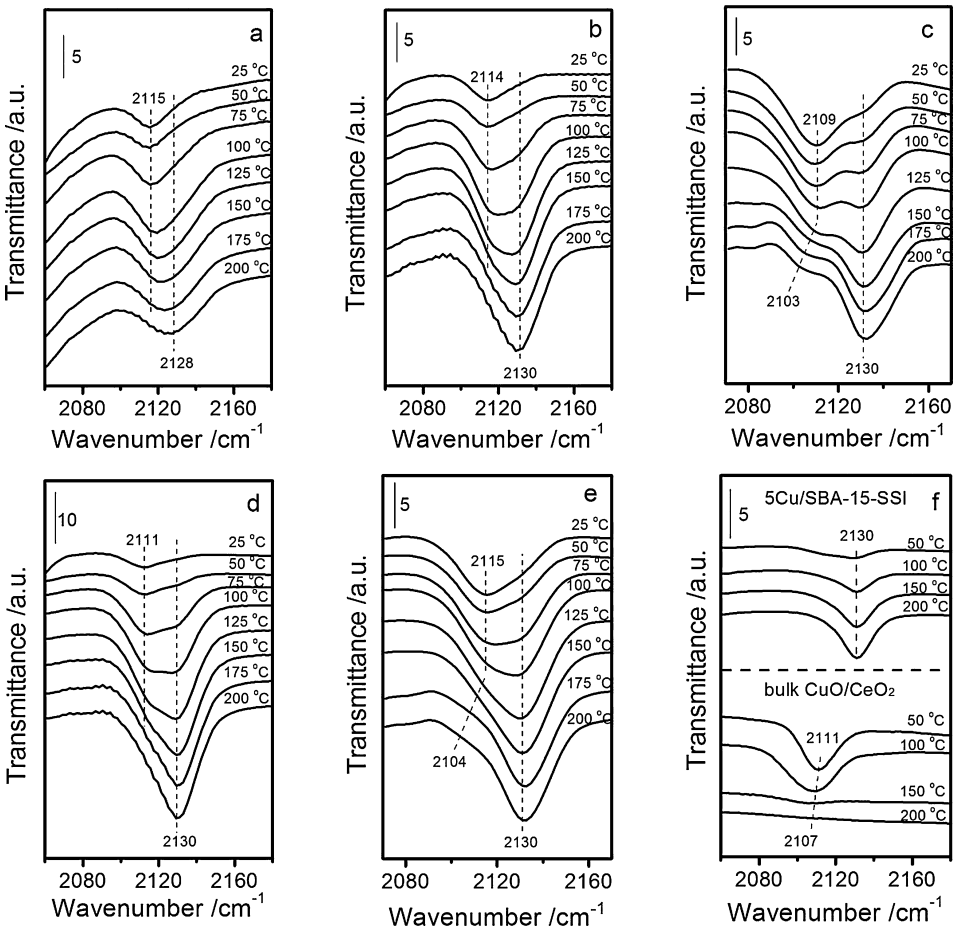

Fig. 5. FT-IR spectra of CO adsorption at various temperatures for (a–d) *x*CuCe/SBA-15-SSI with copper contents of (a) 1 wt%, (b) 3 wt%, (c) 5 wt%, (d) 10 wt%, (e) 5CuCe/SBA-15-WI and (f) 5Cu/SBA-15-SSI, bulk CuO/CeO_2.

of copper species is changed when ceria is used as a carrier. For bulk CuCe sample, the reduction shifts to lower temperatures and two well-resolved H_2 consumption peaks are detected. That is, a small peak (denoted as α) with H_2 consumption maximum at 117 °C and a much larger H_2 consumption peak (denoted as β) with central temperature at 152 °C. According to previous studies, the α and β peaks can be assigned to interfacial copper species in close contact with ceria and the remaining CuO species less associated with ceria, respectively [8,10,37–39].

After introduction of SBA-15, the reduction of copper-ceria catalysts is further changed, as evidenced by the appearance of three consecutive H_2 consumption peaks. For 5CuCe/SBA-15-SSI and 5CuCe/SBA-15-WI, the first two peaks lie in the temperature range between 140 °C and 180 °C, and they just fall into the region (zone I as framed in the figure) corresponding to reduction of copper supported on ceria. The third peak shifts to higher temperatures and can be filed into the temperature range of highly dispersed copper species on SBA-15 (zone II as framed in the figure). Similarly, the

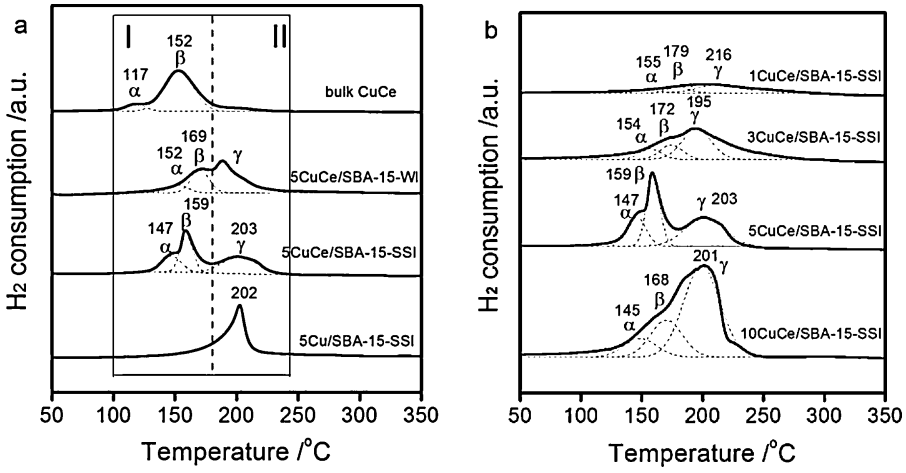

Fig. 6. H_2-TPR profiles of various samples (a) from different method and (b) with varied copper loadings.

reductions of *x*CuCe/SBA-15-SSI with different copper contents can also be deconvoluted into three peaks (Fig. 6b). The first two peaks (α and β) are responsible for reduction of copper species on ceria, while the third peak (denoted as γ) actually reflects the reduction of CuO on SBA-15. Combined with FT-IR results of CO adsorption, it can be safely concluded that irrespective of preparation methods or copper contents, copper species are actually dispersed on both ceria and SBA-15.

By comparing the peak temperatures of various samples, differences are observed on the reducibility of the catalysts as functions of copper loading and preparation method. For *x*CuCe/SBA-15-SSI, both α and β peaks shift to low temperatures with increasing of copper contents, and no further shift is displayed when 10 wt% CuO is loaded. On the other hand, the reduction temperatures of α and β peaks for 5CuCe/SBA-15-SSI are lower than those for 5CuCe/SBA-15-WI, implying the reduction occurs more easily in the sample prepared by the solid state impregnation. As revealed by XPS results, the redox cycle between Cu^{2+}/Cu^{+} and Ce^{3+}/Ce^{4+} is more facile to occur in 5CuCe/SBA-15-SSI than in 5CuCe/SBA-15-WI, which subsequently brings a stronger synergetic interaction between copper and ceria. According to our previous study, the strong synergetic effect between copper and ceria can facilitate the reduction of CuO-CeO_2 [27]. Thus, the reduction behavior of CuO-CeO_2/SBA-15 can be improved by employing the solid state impregnation.

To further reveal the quantitative aspect of copper species on both carriers, the peak areas of H_2-TPR patterns are integrated and the actual H_2 consumptions are calculated by referring to a pure CuO sample. The results are listed in Table 2. It can be clearly seen that for all catalysts, the actual H_2 consumptions (denoted as *A*) are larger than what is needed for the stoichiometric reduction of CuO to metallic Cu (theoretical H_2 consumption, denoted as *T*), suggesting the surface layer of ceria is simultaneously reduced with copper species [40]. As reported elsewhere, the reduction of pure ceria started at temperature higher than 500 °C [41]. The obviously promoted reduction of ceria proves synergetic interaction between copper species and ceria. By comparing *A*/*T* values, valuable information is obtained: (1) the *A*/*T* values vary with copper contents. It displays a volcano-type behavior, with 3 wt% and 5 wt% CuO acquiring largest A/T (*ca.* 1.20), suggesting too much or little copper is not beneficial to enhance copper-ceria interaction; (2) in comparison with wet impregnation, the solid state impregnation shows larger *A*/*T* value, indicating enhanced interaction between copper and ceria is achieved in the absent of solvent. This also corroborates XPS result.

From Table 2, it can also be noticed that the ratios of interfacial CuO (R_{IC}) in supported copper-ceria catalysts are much higher than that in bulk CuO-CeO_2 catalyst. It is reasonable by taking into consideration of the distinct smaller particle size of ceria for CuO-CeO_2/SBA-15 catalysts. Assuming other conditions to be identical, the smaller the particle size is, the more Ce^{3+} and oxygen vacancy is available and the more anchoring sites for copper species, which brings about much more interfacial CuO. In addition to ceria size, it is notable that the preparation method also exerts an essential influence on R_{IC}, with 5CuCe/SBA-15-SSI achieving higher R_{IC} than that of 5CuCe/SBA-15-WI.

The percentage of copper dispersed on ceria (Cu_{CeO_2}) is a fundamental issue for CuO-CeO_2/SBA-15 catalyst system and paramount to the final catalytic performance. By subtracting H_2 consumption of copper on SBA-15 (peak γ) from theoretical H_2 consumption, the H_2 consumption of copper on ceria as well as Cu_{CeO_2} is determined. In principle, for all CuO-CeO_2/SBA-15 catalysts, more than half of copper species are dispersed on mesoporous silica, which should be related to the large surface area of SBA-15. The Cu_{CeO_2} is initially increased with copper contents, and reaches maximum when 5 wt% CuO is introduced. Further increase CuO content to 10 wt% leads to decline of Cu_{CeO_2} from 43.4% to 34.1%. This may be another factor accounting for the lower A/T value at 10 wt% CuO loading. On the other hand, it is important to notice that by replacing wet impregnation with solid state impregnation, the Cu_{CeO_2} can be greatly increased. That is to say, the catalyst from solid state impregnation owns the advantage of distributing more copper species onto ceria, despite the inevitable dispersion of copper species on silica matrix.

Based on the above characterization results, the distributions of copper species in CuO-CeO_2/SBA-15 catalysts are constructed and a representative illustration for the samples from solid state impregnation and wet impregnation is shown in Fig. 7. Most of ceria are confined in mesopores for the two impregnation methods, while the distribution of dispersed copper species is not the same. As the most used method for distributing guest species, wet impregnation is capable of introducing active phases onto porous matrix, and this is validated by copper-ceria in the present study. However, previous studies also proposed that in preparation of CuO/SiO_2 catalysts *via* wet impregnation, the evaporation of solvent during drying step would cause random distribution of copper species [42,43]. Similarly, for SBA-15 supported CuO, it is reported that a certain amount of CuO were essential on the exterior of mesopores [44], and this is also revealed by XPS surface composition result in the present study. The advent of exterior copper species will certainly reduce their contact with ceria confined in the mesopores. On the other hand, certain kind of metal nitrates can be introduced into the porous matrix through melt infiltration [15,45]. In the present case, it is highly possible that both solid state metal precursors (cupric nitrate and cerium nitrate) turn into molten salts when the temperatures reach their melting points. Owing to the mobility of molten salts, the dry precursors can be sucked into the mesopores with the aid of capillary imbibition. Importantly, due to the absence of solvent, the redistribution of copper species can be greatly inhibited, which offers an effective way to increase the chance of copper species in contact with ceria. Moreover, on the basis of XPS and H_2-TPR quantitative calculation results, it seems that in the absence of solvent, the interaction between copper and ceria is more favorable, which generates more Ce^{3+} and higher concentration of interfacial copper species. Both the above mentioned two points are vital for multiple components supported catalysts, as more often than not, the effective contact between promoter and active species is essential for the occurrence of cooperative effect, which governs the final catalytic performance. Thus, from the above preliminary discussion, such unique properties like enhanced interaction between copper and ceria exhibited in CuO-CeO_2/SBA-15 system, are supposed to be also available in fabrication of multi-component catalysts, potentially ensuring solid state impregnation a promising method for fabrication of heterogeneous catalysts.

3.7. The catalytic performances in CO-PROX reaction

Fig. 8a and b show the catalytic performances of *x*CuCe/SBA-15-SSI catalysts in CO-PROX. It is obvious that the CO conversion in rich H_2 is closely associated with copper contents. When 1 wt% Cu is involved, it displays the worst activity, with the maximum CO conversion of 90.1% at 180 °C. Increasing CuO loading from 1 wt% to 3 wt% and 5 wt% leads to remarkable increase in the catalytic activity, further increasing the loading to 10 wt% do not result in corresponding enhancement in the activity. Contrarily, it can be seen that both CO conversion and CO_2 selectivity are significantly decreased at elevated temperatures when the CuO loading is increased to 10 wt%, indicating that a higher CuO loading is more effective for accelerating the H_2 oxidation. As a result, the efficiency for CO conversion is lowered [46].

The CO-PROX curves of bulk CuCe, 5CuCe/SBA-15-SSI and 5CuCe/SBA-15-WI are presented in Fig. 8c and d. The activity of bulk

Table 2
A summary of H_2 consumption and distribution of copper species for various copper-ceria catalysts.

Catalyst	H_2 consumption (μmol)					A/T[a]	Cu_{CeO_2} (%)[b]	R_{IC}[c]
	Actual	α	β	γ	Theoretical			
1CuCe/SBA-15-SSI	2.55	0.21	0.43	1.91	2.38	1.07	19.7	0.33
3CuCe/SBA-15-SSI	8.36	1.12	1.63	5.61	7.14	1.17	21.4	0.41
5CuCe/SBA-15-SSI	14.15	2.73	4.68	6.74	11.90	1.19	43.4	0.37
10CuCe/SBA-15-SSI	25.46	3.10	5.96	16.40	23.80	1.07	31.1	0.34
5CuCe/SBA-15-WI	13.00	1.23	3.16	8.61	11.90	1.09	25.4	0.28
bulk CuCe	12.34	1.47	10.87	–	11.90	1.06	–	0.12

[a] The ratio of actual H_2 consumption to theoretical H_2 consumption.
[b] The percentage of copper dispersed on ceria, which is calculated by $(T-\gamma)/T \times 100\%$.
[c] The ratio of interfacial copper, which is calculated by $\alpha/(\alpha+\beta)$.

CuCe catalyst is comparable to previous study [3] and it exhibits the lowest catalytic activity among the three catalysts. Both the CO conversion and CO_2 selectivity are greatly improved when copper-ceria entities are loaded onto SBA-15, which proves that the supported copper-ceria configuration is advantageous for enhancement of CO-PROX performance. For 5CuCe/SBA-15-WI, although the CO conversion at 100 °C is lower than that of bulk CuO-CeO_2 and only gives 70% conversion of CO, it achieves comparable value at 110 °C and better performance at higher temperatures. Besides, the CO_2 selectivity is also superior to that of bulk CuCe below 160 °C, with a temperature gap about 10 °C to attain the similar hydrogen oxidation activity.

In comparison with bulk CuCe and 5CuCe/SBA-15-WI catalysts, both the CO conversion and operation window corresponding to minimum acceptable CO (100 ppm) of 5CuCe/SBA-15-SSI are greatly improved. More than 99% of CO is converted to CO_2 at temperature as low as 120 °C, and the conversion is still constant until the temperature is raised to 180 °C. As well, the effect of CO_2 and H_2O is investigated. The catalytic performance and long term stability are displayed (Fig. 9). Both 5CuCe/SBA-15-SSI and 5CuCe/SBA-15-WI exhibit a decrease of activity after introduction of CO_2 and H_2O, suggesting the adverse effect of CO_2 and H_2O [47]. Instead, the CO_2 selectivity at elevated temperatures (>120 °C) is improved under full gas composition, which is in agreement with previous reports [5,48,49] and suggests that in addition to CO oxidation, the H_2 oxidation is also inhibited in the presence of CO_2 and H_2O, probably as a result of the blockage of active sites by adsorbed CO_2 and H_2O. It is observed that the 5CuCe/SBA-15-SSI catalyst still get better activity over 5CuCe/SBA-15-WI. Despite with lowered CO conversion, the catalyst own good stability, as revealed by the long term test result (Fig. 9c).

The Arrhenius plots for CO oxidation reaction are displayed in Fig. 10. It can be found that although with different activities, all catalysts display the similar apparent activation energies ($E_{app} = 55 \pm 5$ kJ/mol), which are comparable to literature reports [50–52] and suggests the possible similar reaction route. To date, substantial investigations on CO-PROX reaction over CuO-CeO_2 catalysts have been operated, and insightful information is acquired. It is commonly agreed that, the optimum catalytic property for CO oxidation is achieved in the presence of well dispersed copper oxide patches over ceria nanoparticles [8,10,34]. This has been recently rationalized by spectroscopic analysis under reaction conditions of catalysts, showing that active sites for CO-PROX reaction are related to interfacial copper oxide which is closely contacted with ceria [53]. These interfacial copper are facile to be reduced to Cu^+ during the course of interaction with reactant mixtures, and the newly formed Cu^+ act as adsorption and oxidation sites for CO.

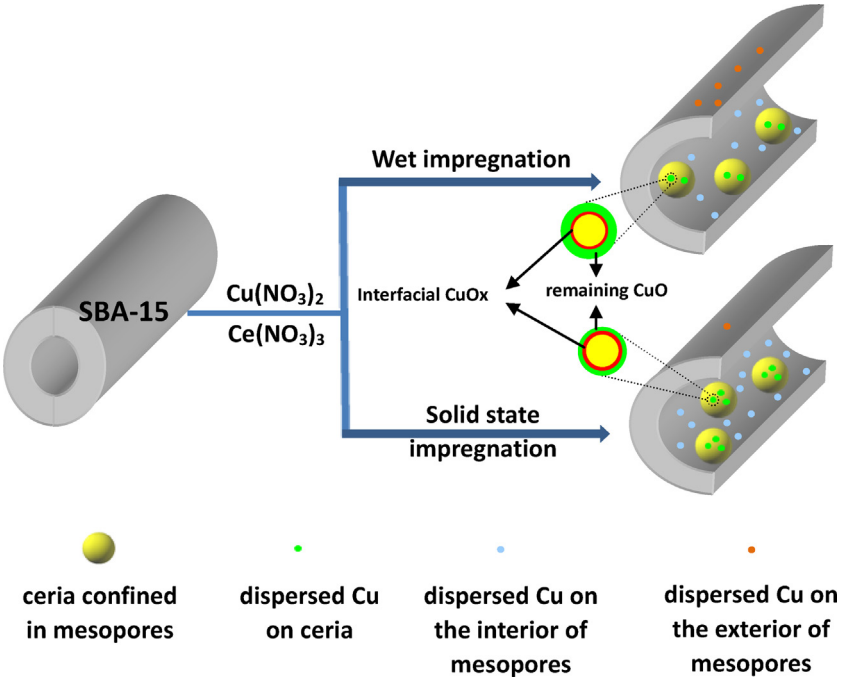

Fig. 7. Schematic illustration of copper species in the samples prepared from solid state impregnation and wet impregnation.

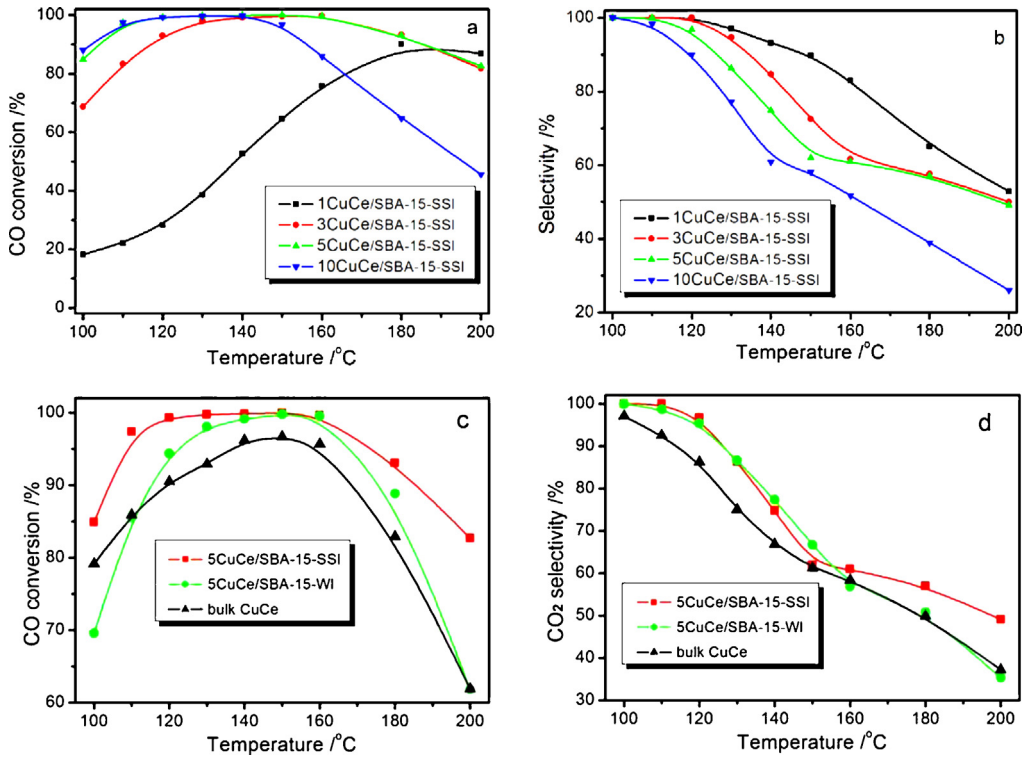

Fig. 8. Catalytic performances as a function of reaction temperatures over indicated catalysts. (a and c) CO conversion, (b and d) CO_2 selectivity.

Hence, it is supposed that in order to get good performance, at least two points should be seriously considered. One is particle size of ceria and the other is effective contact between copper and ceria, both of which are intimately related to the density of active sites. It was reported that the structural, chemical and electronic properties of nanosized ceria were much different from the bulk ceria [54,55]. In the present CuO-CeO_2 system, one notable characteristic for nanosized ceria is the obvious increment of Ce^{3+}

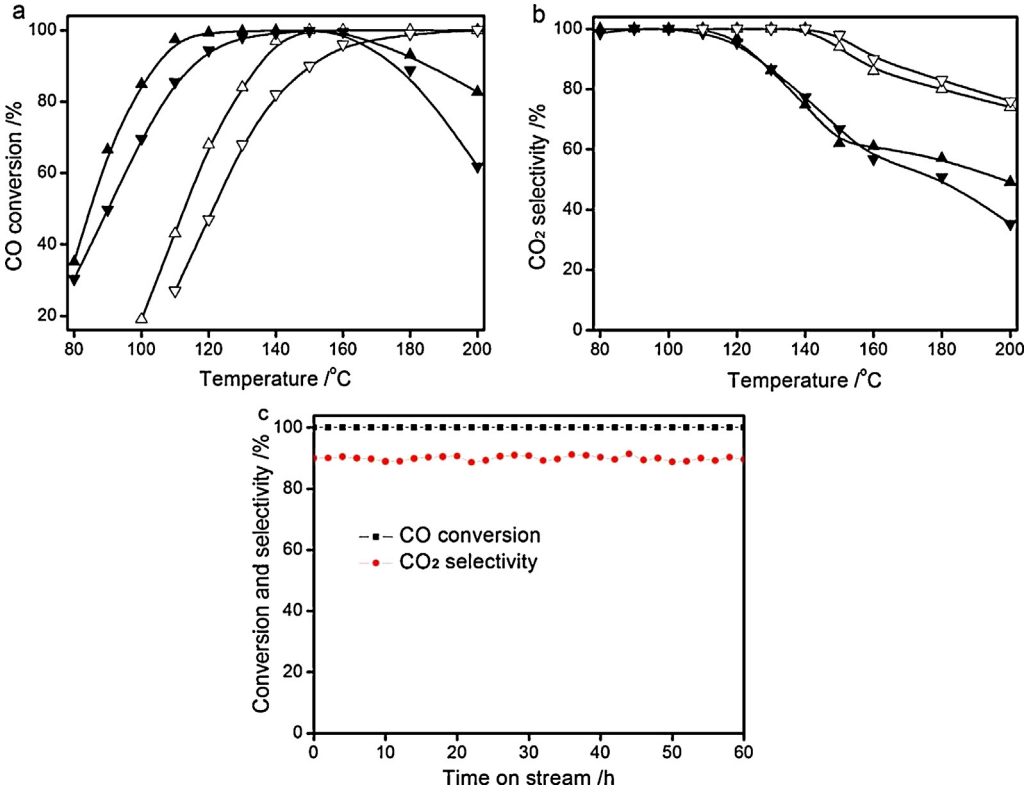

Fig. 9. (a) CO conversion and (b) CO_2 selectivity of 5CuCe/SBA-15-SSI (triangle up) and 5CuCe/SBA-15-WI (triangle down) catalysts. Solid and open symbols denote, respectively, absence and presence of 15% CO_2 and 10% H_2O in the reaction stream. (c) The stability of 5CuCe/SBA-15-SSI in the presence of 15% CO_2 and 10% H_2O at 160 °C.

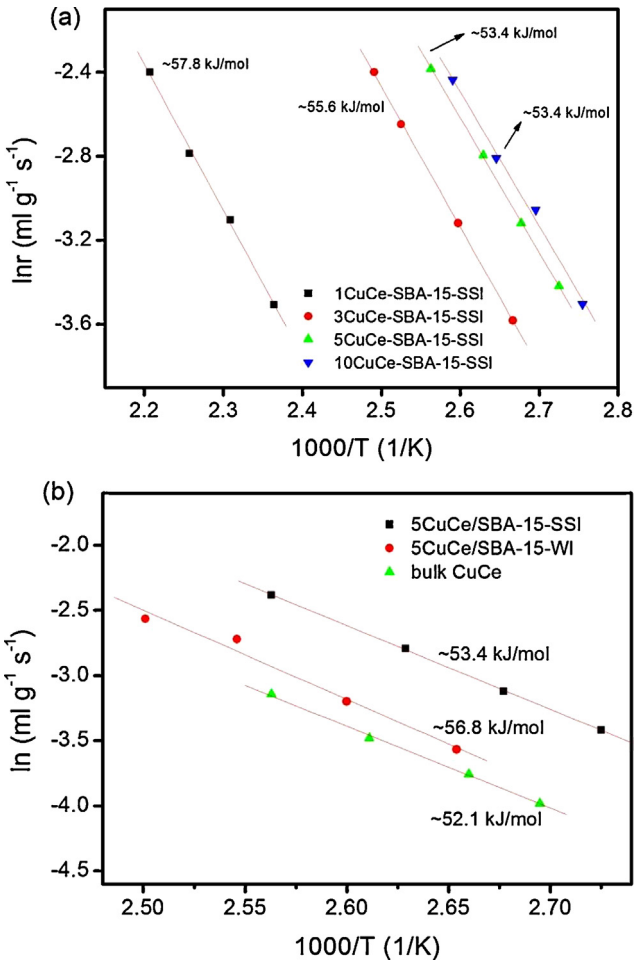

Fig. 10. Arrhenius plots for CO oxidation (under CO-PROX mixture without CO_2 and H_2O) over indicated catalysts.

concentration. As a form of structure defect, these Ce^{3+} are supposed to be directly linked to oxygen vacancy, and Cu^{+} can be induced and stabilized by Ce^{3+} *via* electron transfer between copper and ceria. Thus, by decreasing ceria particle sizes, the number of active sites (Cu^{+}-□-Ce^{3+}) is increased, which leads to higher total rates and higher conversions. This can explain well the great enhancement of catalytic activity of supported copper-ceria system, in comparison with the common bulk CuO-CeO_2 catalyst.

The effective contact between CuO and ceria becomes pivotal for supported copper-ceria system, as some of copper species are actually dispersed on the incoming carrier (silica) and they contribute little to CO conversion. As validated by H_2-TPR result, the solid state impregnation has the advantage of introducing more copper species onto ceria. As well, the interaction between unit copper and ceria is enhanced, which produces higher Ce^{3+} and the related Cu^{+}. These may be the origin of the improved CO-PROX activity of 5CuCe/SBA-15-SSI over its counterpart from the wet impregnation method.

4. Conclusions

In summary, a facile solid state impregnation method was reported to prepare highly active CuO-CeO_2/SBA-15 catalyst for CO-PROX. Both CuO and ceria are well dispersed and the employment of SBA-15 leads to obvious reduction of ceria size and increase of Ce^{3+} concentration, which is advantageous for CO-PROX performance. The copper species are actually dispersed on both carriers, *i.e.* SBA-15 and ceria, as evidenced by FT-IR of CO adsorption and H_2-TPR results. By comparing with CuO-CeO_2/SBA-15 catalyst from wet impregnation, it is observed that the catalyst prepared by solid state impregnation displays such advantages like increased amount of copper-ceria entities and enhanced interaction between CuO and CeO_2, which eventually increases the active sites and upgrades the performance for CO-PROX. On the basis of the present study, it is believed the solid state impregnation will find promising application in fabricating multi-component catalysts, and further study concerning on this aspect is ongoing.

Acknowledgements

The financial supports of National Basic Research Program of China (2010CB732300, 2009CB623500), National Nature Science Foundation of China (20973091), Open Project Program of the State Key Laboratory of Physical Chemistry of Solid Surfaces of Xiamen University (201207), Jiangsu Province Science and Technology Support Program (Industrial, BE2011167) and Jiangsu Planned Projects for Postdoctoral Research Funds (1102027C) are gratefully acknowledged.

References

[1] T.V. Choudhary, D.W. Goodman, Catal. Today 77 (2002) 65–78.
[2] N. Bion, F. Epron, M. Moreno, F. Mariño, D. Duprez, Top. Catal. 51 (2008) 76–88.
[3] G. Avgouropoulos, T. Ioannides, H.K. Matralis, J. Batista, S. Hocevar, Catal. Lett. 73 (2001) 33–40.
[4] G. Avgouropoulos, T. Ioannides, C. Papadopoulou, J. Batista, S. Hocevar, H.K. Matralis, Catal. Today 75 (2002) 157–167.
[5] Y. Liu, Q. Fu, M. Flytzani-Stephanopoulos, Catal. Today 93–95 (2004) 241–246.
[6] D. Gamarra, G. Munuera, A.B. Hungría, M. Fernández-García, J.C. Conesa, P.A. Midgley, X.Q. Wang, J.C. Hanson, J.A. Rodríguez, A. Martínez-Arias, J. Phys. Chem. C 111 (2007) 11026–11038.
[7] R. Kydd, D. Ferri, P. Hug, J. Scott, W.Y. Teoh, R. Amal, J. Catal. 277 (2011) 64–71.
[8] G. Avgouropoulos, T. Ioannides, Appl. Catal. A: Gen. 244 (2003) 155–167.
[9] W. Liu, M. Flytzani-Stephanopoulos, J. Catal. 153 (1995) 304–316.
[10] L.C. Chung, C.T. Yeh, Catal. Commun. 9 (2008) 670–674.
[11] C.R. Jung, A. Kundu, S.W. Nam, H.I. Lee, Appl. Catal. B: Environ. 84 (2008) 426–432.
[12] A. Hornés, A.B. Hungría, P. Bera, A. Lopez Cámara, M. Fernandez-García, A. Martínez-Arias, L. Barrio, M. Estrella, G. Zhou, J.J. Fonseca, J.C. Hanson, J.A. Rodriguez, J. Am. Chem. Soc. 132 (2010) 34–35.
[13] V. Ramaswamy, S. Malwadkar, S. Chilukuri, Appl. Catal. B: Environ. 84 (2008) 21–29.
[14] G. Aguila, F. Gracia, P. Araya, Appl. Catal. A: Gen. 343 (2008) 16–24.
[15] T.M. Eggenhuisen, J.P. den Breejen, D. Verdoes, P.E. de Jongh, K.P. de Jong, J. Am. Chem. Soc. 132 (2010) 18318–18325.
[16] A.K. Medina-Mendoza, M.A. Cortés-Jácome, J.A. Toledo-Antonio, C. Angeles-Chávez, E. López-Salinas, I. Cuauhtémoc-López, M.C. Barrera, J. Escobar, J. Navarrete, I. Hernández, Appl. Catal. B: Environ. 106 (2011) 14–25.
[17] C.J. Tang, H.L. Zhang, C.Z. Sun, J.C. Li, L. Qi, Y.J. Quan, F. Gao, L. Dong, Catal. Commun. 12 (2011) 1075–1078.
[18] D.Y. Zhao, J.L. Feng, Q.S. Huo, N. Melosh, G.H. Fredrickson, B.F. Chmelka, G.D. Stucky, Science 279 (1998) 548–552.
[19] X.Y. Wang, Q. Kang, D. Li, Appl. Catal. B: Environ. 86 (2009) 166–175.
[20] L. Dong, Y.S. Jin, Y. Chen, Sci. China: Ser. B 40 (1997) 24–30.
[21] K.S.W. Sing, D.H. Everett, R.A.W. Haul, L. Moscou, R.A. Pierotti, J. Rouquerol, T. Siemieniewska, Pure Appl Chem. 57 (1985) 603–619.
[22] J.C. Groen, L.A.A. Peffer, J. Pérez-Ramirez, Micropor. Mesopor. Mater. 60 (2003) 1–17.
[23] P. Van Der Voort, P.I. Ravikovitch, K.P. De Jong, A.V. Neimark, A.H. Janssen, M. Benjelloun, E. Van Bavel, P. Cool, B.M. Weckhuysen, E.F. Vansant, Chem. Commun. (2002) 1010–1011.
[24] M. Alifanti, B. Baps, N. Blangenois, J. Naud, P. Grange, B. Delmon, Chem. Mater. 15 (2003) 395–403.
[25] F. Zhang, P. Wang, J. Koberstein, S. Khalid, S.W. Chan, Surf. Sci. 563 (2004) 74–82.
[26] S.S. Lee, H.G. Zhu, E.Q. Contreras, A. Prakash, H.L. Puppala, V.L. Colvin, Chem. Mater. 24 (2012) 424–432.
[27] L. Qi, Q. Yu, Y. Dai, D.J. Tang, L.J. Liu, H.L. Zhang, F. Gao, L. Dong, Y. Chen, Appl. Catal. B: Environ. 119–120 (2012) 308–320.
[28] H.J. Li, G.S. Qi, Tana, X.J. Zhang, X.M. Huang, W. Li, W.J. Shen, Appl. Catal. B: Environ. 103 (2011) 54–61.
[29] R.K. Hailstone, A.G. DiFrancesco, J.G. Leong, T.D. Allston, K.J. Reed, J. Phys. Chem. C 113 (2009) 15155–15159.
[30] A.B. Kehoe, D.O. Scanlon, G.W. Watson, Chem. Mater. 23 (2011) 4464–4468.
[31] N. Michael, J. Phys. Chem. C 115 (2011) 6671–6681.
[32] A. Tschope, W. Liu, M. Flytzani-Stephanopoulos, J.Y. Ying, J. Catal. 157 (1995) 42–50.

[33] J.F. Moulder, W.F. Stickle, P.E. Sobol, K.D. Bomben, Handbook of X-Ray Photoelectron Spectroscopy, Perkin-Elmer Corporation, Physical Electronics Division, Eden Prairie, MN, 1993.
[34] C.S. Polster, H. Nair, C.D. Baertsch, J. Catal. 266 (2009) 308–319.
[35] K.I. Hadjiivanov, G.N. Vayssilov, Adv. Catal. 47 (2002) 307–511.
[36] A. Hornes, P. Bera, A.L. Camara, D. Gamarra, G. Munuera, A. Martinez-Arias, J. Catal. 268 (2009) 367–375.
[37] M.F. Luo, Y.J. Zhong, X.X. Yuan, X.M. Zheng, Appl. Catal. A: Gen. 162 (1997) 121–131.
[38] L. Kundakovic, M. Flytzani-Stephanopoulos, Appl. Catal. A: Gen. 171 (1998) 13–29.
[39] R. Si, J. Raitano, N. Yi, L.H. Zhang, S.W. Chan, M. Flytzani-Stephanopoulos, Catal. Today 180 (2012) 68–80.
[40] L. Ilieva, G. Pantaleo, I. Ivanov, A.M. Venezia, D. Andreeva, Appl. Catal. B: Environ. 65 (2006) 101–109.
[41] P. Zimmer, A. Tschope, R. Birringer, J. Catal. 205 (2002) 339–345.
[42] A.J. van Dillen, R.J.A.M. Terorde, D.J. Lensveld, J.W. Geus, K.P. de Jong, J. Catal. 216 (2003) 257–264.
[43] T. Toupance, M. Kermarec, C. Louis, J. Phys. Chem. B 104 (2000) 965–972.
[44] L.F. Chen, P.J. Guo, L.J. Zhu, M.H. Qiao, W. Shen, H.L. Xu, K.N. Fan, Appl. Catal. A: Gen. 356 (2009) 129–136.
[45] W.B. Yue, W.Z. Zhou, Chem. Mater. 19 (2007) 2359–2363.
[46] B.T. Qiao, A.Q. Wang, J. Lin, L. Li, D.S. Su, T. Zhang, Appl. Catal. B: Environ. 105 (2011) 103–110.
[47] D. Gamarra, A. Martinez-Arias, J. Catal. 263 (2009) 189–195.
[48] W. Liu, M. Flytzani-Stephanopoulos, J. Catal. 153 (1995) 317–332.
[49] G. Sedmak, S. Hočevar, J. Levec, J. Catal. 213 (2003) 135–150.
[50] M. Moreno, G.T. Baronetti, M.A. Laborde, F.J. Mariño, Int. J. Hydrogen Energy 33 (2008) 3538–3542.
[51] D.H. Kim, J.E. Cha, Catal. Lett. 86 (2003) 107–117.
[52] D. Gamarra, M. Fernández-Garacia, C. Belver, A. Martínez-Arias, J. Phys. Chem. C 114 (2010) 18576–18582.
[53] D. Gamarra, C. Belver, M. Fernández-Garcia, A. Martínez-Arias, J. Am. Chem. Soc. 129 (2007) 12064–12065.
[54] L.J. Wu, H.J. Wiesmann, A.R. Moodenbaugh, R.F. Klie, Y.M. Zhu, D.O. Welch, M. Suenaga, Phys. Rev. B 69 (2004) 125415.
[55] J.H. Xu, J. Harmer, G.Q. Li, T. Chapman, P. Collier, S. Longworth, S.C. Tsang, Chem. Commun. 46 (2010) 1887–1889.